Electronic Research Archive

http://www.aimspress.com/journal/ERA

ERA, 31(6): 3200–3217.
DOI: 10.3934/era.2023162
Received: 02 January 2023
Revised: 19 January 2023
Accepted: 01 February 2023
Published: 27 March 2023

Research article

Anas platyrhynchos optimizer with deep transfer learning-based gastric cancer classification on endoscopic images

Mashael S. Maashi[1], Yasser Ali Reyad Ali[2], Abdelwahed Motwakel[3,*], Amira Sayed A. Aziz[4], Manar Ahmed Hamza[5] and Amgad Atta Abdelmageed[5]

[1] Department of Software Engineering, College of Computer and Information Science, King Saud University, PO Box 103786, Riyadh 11543, Saudi Arabia
[2] Department of Information System, College of Computer and Information Science, King Saud University, PO Box 103786, Riyadh 11543, Saudi Arabia
[3] Department of Information Systems, College of business administration in Hawtat bani Tamim, Prince Sattam bin Abdulaziz University, Saudi Arabia
[4] Department of Digital Media, Faculty of Computers and Information Technology, Future University in Egypt, New Cairo 11835, Egypt
[5] Department of Computer and Self Development, Preparatory Year Deanship, Prince Sattam bin Abdulaziz University, Al-Kharj, Saudi Arabia

* **Correspondence:** Email: am.ismaeil@psau.edu.sa.

Abstract: Gastric Cancer (GC) has been identified as the world's fifth most general tumor. So, it is important to diagnose the GC at initial stages itself to save the lives. Histopathological analysis remains the gold standard for accurate diagnosis of the disease. Though Computer-Aided Diagnostic approaches are prevalently applied in recent years for the diagnosis of diseases, it is challenging to apply in this case, due to the lack of accessible gastric histopathological image databases. With a rapid progression in the Computer Vision (CV) technologies, particularly, the emergence of medicinal image classifiers, it has become feasible to examine all the types of electron micrographs in a rapid and an effective manner. Therefore, the current research article presents an Anas Platyrhynchos Optimizer with Deep Learning-based Gastric Cancer Classification (APODL-GCC) method for the classification of GC using the endoscopic images. The aim of the proposed APODL-GCC method is to identify the presence of GC with the help of CV and Deep Learning concepts. Primarily, the APODL-GCC technique employs a contrast enhancement technique. Next, the feature extraction process is performed using a neural architectural search network model to generate a collection of feature vectors. For

hyperparameter optimization, the Anas Platyrhynchos Optimizer (APO) algorithm is used which enhances the classification performance. Finally, the GC classification process is performed using the Deep Belief Network method. The proposed APODL-GCC technique was simulated using medical images and the experimental results established that the APODL-GCC technique accomplishes enhanced performance over other models.

Keywords: gastric cancer; artificial intelligence; deep learning; computer vision; NASNet model; endoscopic images

1. Introduction

Gastric Cancer (GC) is one of the most commonly-occurring cancerous types across the globe. However, its diagnosis rate is comparatively poor and has become a major threat globally [1]. Malignant tissues may grow in any part of the Gastrointestinal (GI) tract since it gets directly and constantly exposed to carcinogens in the gut environment via food ingestion. Various authors have identified several hotspots for malevolent conversion of the tissues that get continuously exposed to carcinogens. GI tumors cause 35% of the cancer-related mortality and 26% of tumor incidence globally [2]. The current increase in the mortality and incidence rates can be connected to the increasing occurrence of adaptable risk components like unhealthy diet, sedentary lifestyle, other metabolic abnormalities and obesity [3]. The outcomes from the recent analysis have exposed a substantial surge in GI cancer occurrence among the individuals aged between 25 and 49 years, thus warning the public about the evolution of medical complications [4]. The five main GI tumors lead to substantial global problems, such as hepatocellular carcinoma, esophageal squamous cell carcinoma, colorectal cancer, pancreatic cancer and gastric adenocarcinoma [5]. Unfortunately, early diagnosis of the GI-based tumors is frequently missed due to the absence of particular indications. In most of the cases, the medical attention is sought only when non-specific indications turn out to be unbearable [6,7].

With the fast expansion of Computer Vision (CV) technologies, particularly, the development of medical image classifiers, any type of electron microscopic images can be inspected in a rapid and an efficient manner [8]. Therefore, it presents a chance to realize a solution that is relevant to the diagnosis of GC. Particularly, the image classification process serves a significant role in computer-aided diagnostics [9]. The outcomes attained from the image classification approaches are predominantly utilized as significant references by doctors in terms of differentiating the malignant tumors from the benign ones, differentiating the differentiation phases of cancers and distinguishing the subtypes in cancer [10,11]. Moreover, with the progression of medical image classification technology, the main aim is to have a high anti-interference ability and attain the maximum precision.

Computer-related analysis of the tissue images is gaining attention among the researchers in digital pathology [12]. In recent times, Deep Learning (DL) techniques have been leveraged to classify and distinguish different types of cancers including the GC. DL utilizing the Convolutional Neural Network (CNN) systems includes visual recognition capability since it can discern the features directly from large training datasets, thus outpacing the human beings [13]. With the current adoption of digital pathology methods such as the Whole-Slide Imaging (WSI) technique for key prognosis, there is an explosive growth experienced in the digitalized tissue slides. This in turn renders massive volumes of digital pathological images [14,15]. But, the application of DL in digital histopathology is still in a

nascent stage. So, the accuracy and efficacy of the pathology analysis are enhanced by merging the routine digitalization of DL and WSI.

The current research article introduces an Anas Platyrhynchos Optimizer (APO) with DL-based GC classification (APODL-GCC) technique for endoscopic images. The presented APODL-GCC technique employs a contrast enhancement technique. Next, the feature extraction process is performed with the help of Neural Architectural Search network (NASNet) model to generate a collection of feature vectors. For hyperparameter optimization, the APO algorithm is used which enhances the classification performance. Finally, the GC classification process is performed using the Deep Belief Network (DBN) method. The proposed APODL-GCC technique was simulated using the medical images and the outcomes were achieved.

2. Related works

In literature [16], a new publicly-available gastric histopathology sub-size image database (GasHisSDB) was published to determine the performance of the classifiers. In order to prove that the erstwhile image classification techniques have differences on the GasHisSDB, the authors selected various classifiers for evaluation. A new transformer-based classifier, seven conventional machine learning techniques and three CNN classifiers were chosen to validate the image classification tasks. In the study conducted earlier [17], an RF deep feature selection technique was modelled. By compiling the Copy Number Variation (CNV) data and gene expression data, the dimensions of the multi-omics data were minimized and the classification accuracy was improved using a DNN technique and the RF. Li et al. [18] projected a DL-related structure called GT-Net for automatic segmentation of the GC. The devised GT-Net implemented diverse structures for deep and shallow layers for a superior extraction of the features.

Zhu et al. [19] built a CNN-Computer-Aided Diagnostic (CAD) mechanism related to endoscopic images to screen the patients and determine the depth of invasion using endoscopic resection. An Artificial Intelligence (AI)-related CNN-CAD system was advanced in this study with the help of TL through an existing pre-trained CNN architecture i.e., ResNet50. Lee et al. [20] presented a CADx mechanism that differentiates and categorizes the gastric tumors from other pre-cancerous circumstances like gastritis, gastric polyps, bleeding and gastric ulcers. This mechanism leveraged the DL method i.e., Xception which involves depthwise separable convolution for the categorization of non-cancers and cancer. The presented technique had stages such as the fast and robust FCM method for image segmentation during preprocessing stage. These techniques produce a possible technique for differentiation and the classification of tumors from other gastric diseases.

Yoon et al. [21] developed an optimized method for depth prediction and EGC detection. In this study, the authors inspected the elements that hinder the outcomes of AI-based diagnosis. The authors used the Visual Geometry Group (VGG)-16 method to classify the endoscopic images as either non-EGC or EGC (T1a or T1b). To construct a method for the identification of EGC areas during training, the authors devised a new loss function that concurrently measures the localization and classification errors. In the study conducted earlier [22], TL was implemented via a fine-tuned deep CNN technique for mechanical categorization of the M-NBI images into two groups such as the EGC images and normal gastric images. Furthermore, this study also explored the impact of TL upon the classifier's outcome under four aspects such as the size of the network input image, training dataset, basic structures of the deep CNN and the number of optimally-tuned network layers; this study even

presented a certain set of guidelines to be followed in this domain for later studies.

3. Proposed model

In the current research work, a new APODL-GCC approach has been modelled for GC classification on endoscopic images. The presented APODL-GCC technique focuses on the identification of GC using the CV and DL concepts. It comprises a sequence of operations such as the contrast enhancement, feature extraction using the NASNet, APO-based hyperparameter tuning and the DBN classification. Figure 1 illustrates the workflow of the APODL-GCC approach.

3.1. Image preprocessing

Primarily, the APODL-GCC technique exploits the contrast enhancement technique. CLAHE is different from the Adaptive Histogram Equalization (AHE) method it overcomes the over-amplification of the contrast. CLAHE is applied to smaller regions of the image that are termed as tiles, instead of the whole image. The adjacent tiles are subsequently compiled through bilinear interpolation so as to remove the artificial boundary. This method is executed to enrich the image contrast.

3.2. Feature extraction using the optimal NASNet model

At this stage, the feature extraction process is performed with the help of NASNet model to produce a collection of feature vectors. Zoph and Le proposed a neural structure search network, named as the NASNet model. This model uses Reinforcement Learning and Recurrent Neural Network (RNN) technique for training so as to attain the most precise parameters [23]. Constructing a CNN model requires extensive computational time, in case if the content is larger as in the case of ImageNet data. The CNN model searches for a better structure from the smaller data and transmits it so that it can be used for training using the larger dataset. This phenomenon is referred to as learning transferable structure. The NASNet structure is scaled based on the quantity of information.

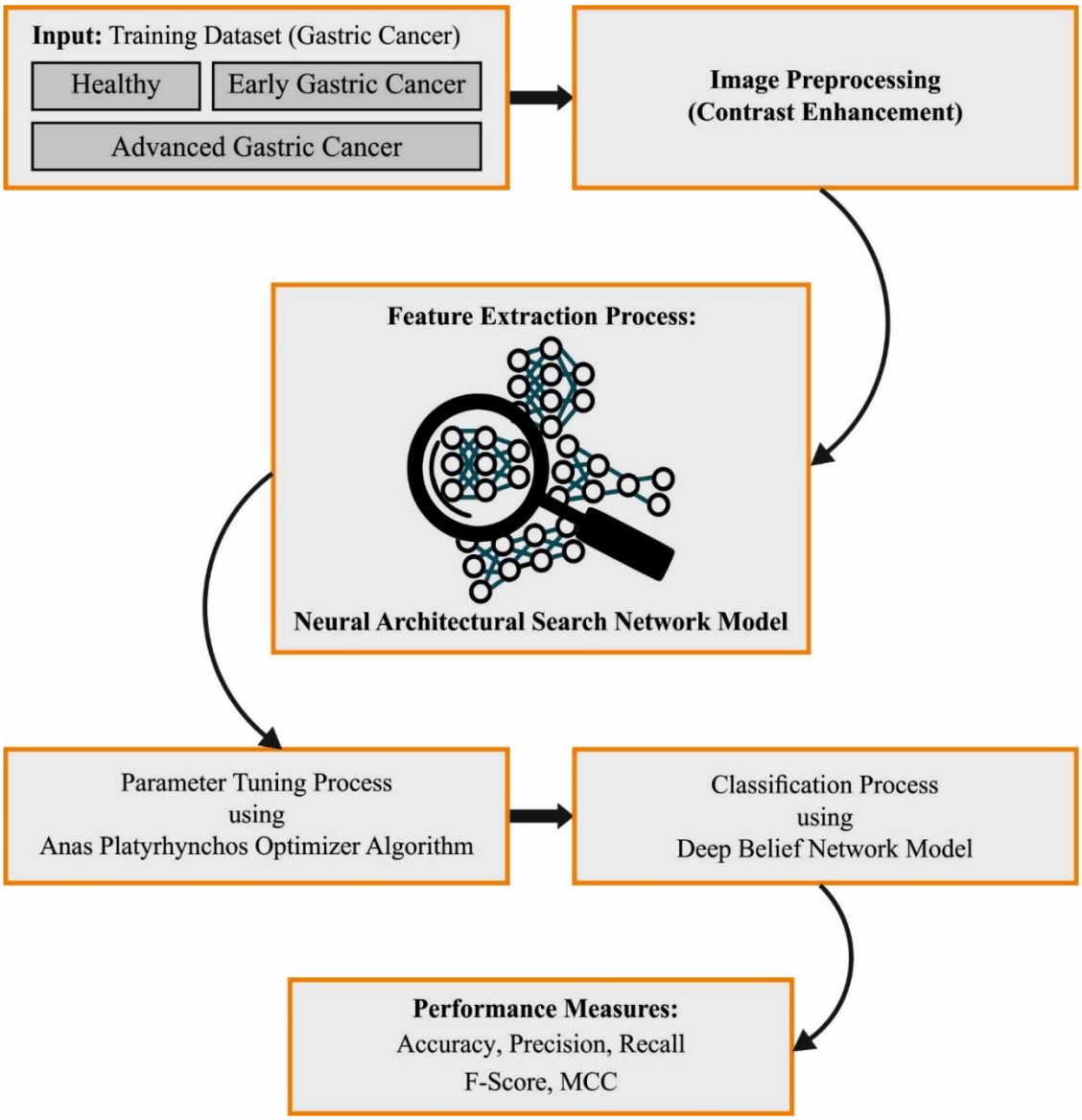

Figure 1. Workflow of the proposed APODL-GCC approach.

Here, N time denotes the time required to identify and segregate the number of cancerous cells from the normal cells. In this stage, the RNN approach is implemented as a search technique. An example operation for detection and classification of the cancerous and normal cells is given below. This is achieved by searching the controller RNN for a proper architecture.

- 1 × 7 then 7 × 1 convolutional layer
- 3 × 3 average pooling layer
- 5 × 5 max pooling layer
- 1 × 1 convolutional layer
- 3 × 3 depth-wise separable convolutional layer
- 7 × 7 depth-wise separable convolutional layer

- 1 × 3 then 3 × 1 convolutional layer
- 3 × 3 dilated convolutional layer
- 3 × 3 max pooling layer
- 7 × 7 max pooling layer
- 3 × 3 convolutional layer
- 5 × 5 depth-wise separable convolutional layer

For hyperparameter optimization, the APO algorithm is used which in turn enhances the classification performance. The population in the APO is established based on the Anas platyrhynchos performance method as given below [24].

$$Pop_i = rand \times (up - low) + low. \tag{1}$$

In Eq (1), Pop_i represents the i^{th} population, N denotes the population size, low and up indicate the lower and upper boundaries of the search space respectively and $rand$ denotes the arbitrary values selected in the range of [0,1]. With regards to warning performance, the fly-in-danger functions are recognized by the selected probability Pc. The basic method of warning classification is established using the following equation:

Step1: Evaluate the probability of distress Pc using the following expression.

$$Pc_i = \frac{rank\big(fit(Pop_i)\big)}{N}. \tag{2}$$

In Eq (2), $fit(Pop_i)$ indicates the fitness value of Pop_i, and $rank\big(fit(Pop_i)\big)$ is considered as a rank of individual Pop_i values among other individuals in the population.

Step2: Once the probability Pc is attained, a novel individual is constructed based on the equation given below.

$$Pop_i(t+1) = Pop_i(t) + sign\left(rand - \frac{1}{2}\right) \times \alpha_0 \times \vee\, Pop_i(t) - Pop_{best}(t) \vee \times Levy(s). \tag{3}$$

Now, t represents the present iteration, Pop_{est} shows the lead duck, $\alpha_0 > 0$ denotes the step length scale factor and $sign$ signifies the sign function. Levy Flight (LF) is responsible for arbitrary walks and the distribution equation is formulated as given below.

$$Levy \sim \mu = t^{-\lambda}, 1 < \lambda \leq 3. \tag{4}$$

LF is a distinct type of arbitrary walk, and the distribution probability of the step length follows a heavy-tailed distribution as given below.

$$s = \frac{\mu}{|\nu|^{\frac{1}{\beta}}}. \tag{5}$$

In Eq (5), s indicates the LF step length. Moreover, $\lambda = 1 + \beta$; also, $\alpha_0 = 0.01$ and $\beta = 3/2$, as CS is fixed. Additionally, μ and ν are selected for the standard distribution $\mu = N\big(0, \delta_\mu^2\big)$ and $\nu = N(0, \delta_\nu^2)$.

$$\delta_{\mu} = \left[\frac{\Gamma(1+\beta) sin\left(\frac{\pi\beta}{2}\right)}{\beta \times \Gamma\left(\frac{1+\beta}{2}\right) \times \frac{2(\beta-1)}{2}} \right]_{\delta_{v}=1}^{\frac{1}{\beta}} \tag{6}$$

An intelligent technique is selected for this study to simulate the biological migration process. Similar to the SOMA, the APO essentially concentrates on the Anas platyrhynchos, thus simulating its migration movement. SOMA and APO differ from each other in terms of place upgrade method and the flow of the technique. In this performance, a basic technique is established as follows.

Step1: Once an optimal particle is defined, then other search particles try to shift towards the best particles which is mathematically expressed as follows:

$$Pop_i(t+1) = Pop_i(t) - A|C \times Pop_{best}(t) - Pop(t)|, \tag{7}$$

In Eq (7), A and C indicate the co-efficient vectors that are obtained as given below.

$$A = 2a \times rand - a, \tag{8}$$

$$C = 2 \times rand, \tag{9}$$

Here, a indicates the co-efficient vector that gets linearly decreased with multiple iterations. The value of a is expressed as follows.

$$a = 2 - t\frac{2}{T} \tag{10}$$

In this expression, T indicates the maximal number of iterations.

Step2: Once the novel individual solution is found to be worse than the older solution, then other particle Pop_{and} is randomly selected

Step 3: When Pop_{and} is better than Pop, then the i^{th} individual is transferred to an arbitrary particle Pop_{and} as given below.

$$Pop_i(t+1) = \left(Pop_{rand}(t) - Pop_i(t)\right) \times e^{-l^2} + Pop_i(t), \tag{11}$$

Now l shows the distance of the arbitrary particles and the i^{th} individual.

Step4: When Pop_{and} corresponds to Pop_i, it remains the same.

Step5: Once the Pop_{rad} is less than Pop_i, then the particle moves towards the i^{th} individual in a random manner using the following expression.

$$Pop_{rand}(t+1) = \left(Pop_i(t) - Pop_{rand}(t)\right) \times e^{-l^2} + Pop_{rand}(t), \tag{12}$$

Fitness selection is an essential feature in APO system. The solution encoded is exploited to calculate the aptitude (goodness) of the candidate solutions. At this point, the accuracy value is the main criterion, employed in this study, to decide the fitness function.

$$Fitness = max(P) \tag{13}$$

$$P = \frac{TP}{TP + FP} \tag{14}$$

Here, TP denotes the True Positive values whereas FP stands for the False Positive value.

3.3. GC classification using DBN

Lastly, the GC classification process is carried out with the help of the DBN model. During the classification process, the normalized feature vector is provided as the input to the DBN mechanism for both detection and the classification of the GC [25]. Artificial Neural Network (ANN) is modeled by dissimilar output and hidden unit layers and is named as DL. It encompasses two levels, namely,

- Pre-training phase
- Fine-tuning phase

Pre-training phase

In DBN technique, an essential feed forward network and a deep structure are involved in which the sample is derived from the input to output layers through the highest quantity of hidden nodes that possess additional nodes. Based on the application of the DBN approach, the algorithm generates the activation function according to the hidden unit that differentiates the DBN method. Moreover, the Restricted Boltzmann Machine (RBM) is defined to resolve the problems encountered in potential activation function. Figure 2 showcases the framework of DBN. RBM is a type of Markov subjective field that encompasses the individual layers with stochastic hidden unit.

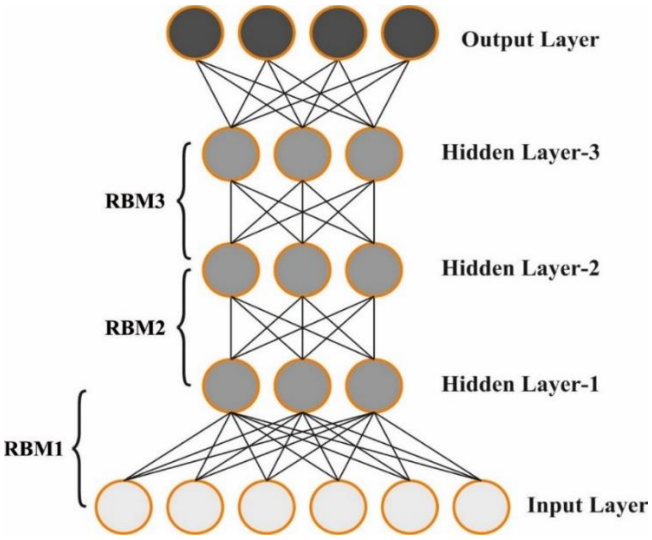

Figure 2. Framework of DBN.

Step 1: Initializing the rich unit v for RBM training.

$$F(v,h) = -\sum_{k=1}^{K}\sum_{l=1}^{L} W_{kl}v_k h_l - \sum_{k=1}^{K}\alpha_k v_k - \sum_{l=1}^{L}\beta_l h_l \tag{15}$$

In Eq (4), W_{kl} indicates the symmetric transmission between the $v_k$visible and h_l hidden layers, the term $\alpha \wedge \beta$ indicates the biases and K and L show the quantity of visible and hidden layers respectively. The subordinate of the log possibility, of the preparation vector, with regards to its weight is irregular. From the hidden unit of RBM, there is no unpredicted replies that tend to accomplish the

impartial sample from $(V_k, h_l)_{data}$.

$$\rho(h_l = 1|v) = \delta\left(\sum_{k=1}^{K} W_{kl} v_k + \alpha_l\right) \tag{16}$$

In Eq (16), $\delta(x)$indicates the logistic sigmoid function, $\frac{1}{(1+exp(x))}$ and $v_k \; and \; h_l$shows the unbiased samples.

Updating phase

The hidden layer is upgraded whereas the visible unit is regarded as a simultaneous element from both visible and the hidden layers. It leads to a complex technique as given below.

$$\Delta W_{kl}\theta(v_k h_l)_{data} - (v_k h_l)_{reconstruction} \tag{17}$$

In Eq (17), the RBM undergoes training whereas the divergent RBM is constructed with a multiple layer approach. In general, different RBMs are stacked together and the visible input unit is identified as a quality measure. The vector for the units are effectively placed in the RBM layer that is shared over the application of shared model in the present weight and bias. Consequently, the final layer is officially trained to secure the RBM. Thereby, the obtained DNN weights are occupied in the fine-tuning phase.

4. Experimental validation

The proposed model was simulated using Python 3.6.5 tool on a PC configured with i5-8600k, GeForce 1050Ti 4GB, 16GB RAM, 250GB SSD, and 1TB HDD. The parameter settings are given as follows: learning rate: 0.01, dropout: 0.5, batch size: 5, epoch count: 50, and activation: ReLU. In this section, the experimental outcomes of the proposed APODL-GCC method were validated using the GC dataset [26]. This dataset has a total of 1500 images as briefed in Table 1. Figure 3 showcases some of the sample images from the dataset. The dataset holds images under three classes with 500 samples under each class.

Table 1. Details of the dataset.

Class	No. of Images
Healthy	500
Early gastric cancer (EGC)	500
Advanced gastric cancer (AGC)	500
Total Number of Images	**1500**

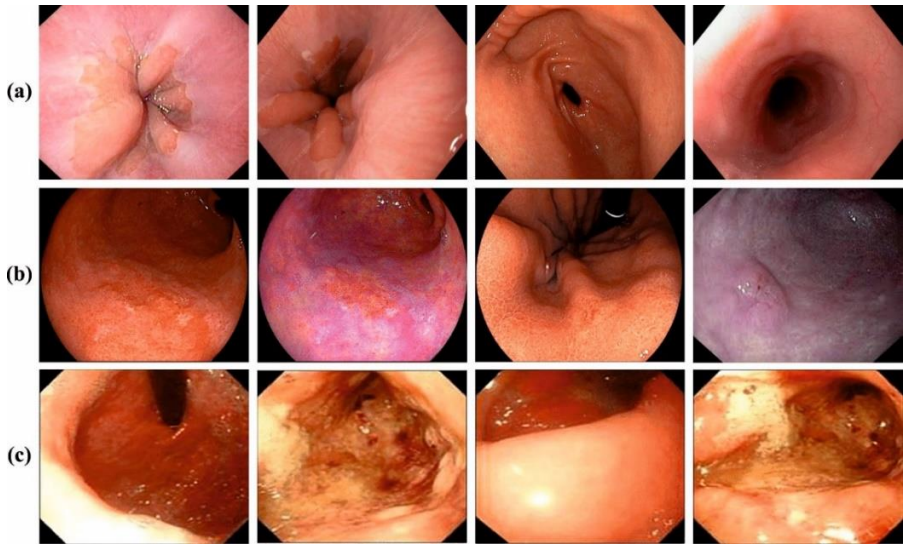

Figure 3. Sample Images a) Healthy b) EGC c) AGC.

The GC classification output of the proposed APODL-GCC model is shown in Figure 4 in the form of confusion matrix. The results infer that the APODL-GCC model accomplished an effectual categorization of the dataset under healthy and GC classes.

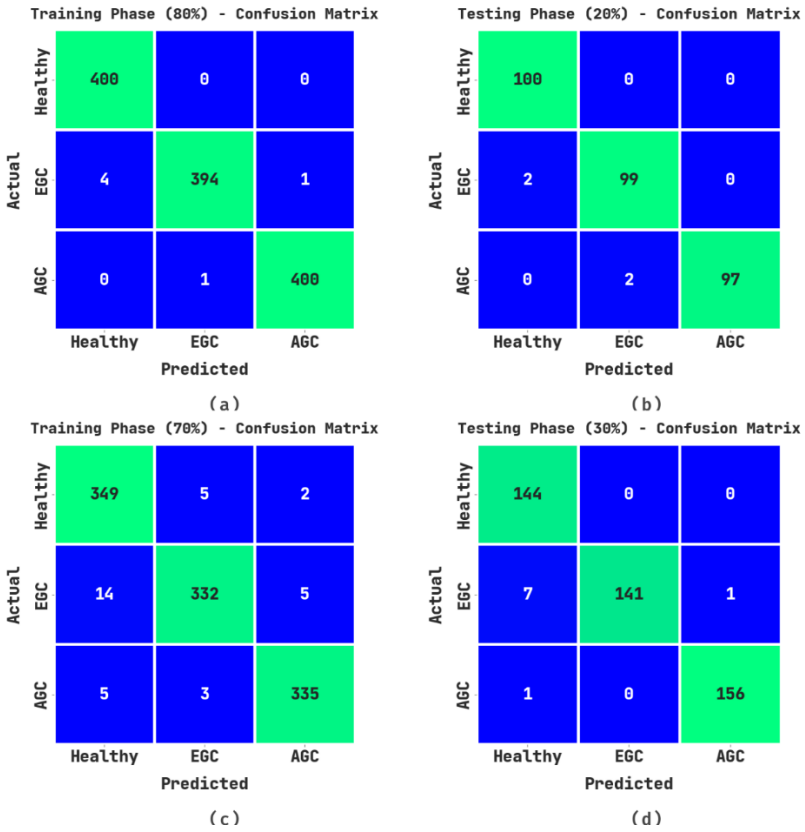

Figure 4. Confusion matrices of the APODL-GCC system (a-b) TR/TS databases of 80: 20 and (c-d) TR/TS databases of 70: 30.

Table 2 and Figure 5 portray the GC classification results accomplished by the proposed APODL-GCC model with 80: 20 of TR/TS databases. The outcomes denote that the APODL-GCC model recognized both healthy and the GC cases accurately. On 80% of TR database, the APODL-GCC model gained an average $accu_y$ of 99.67%, $prec_n$ of 99.50%, $reca_l$ of 99.50%, F_{score} of 99.50%, and an MCC of 99.25%. Meanwhile, on 20% of TS database, the APODL-GCC method obtained an average $accu_y$ of 99.11%, $prec_n$ of 98.69%, $reca_l$ of 98.67%, F_{score} of 98.67%, and an MCC of 98.01%.

Table 2. GC classification outcomes of the APODL-GCC system on 80:20 of TR/TS databases.

Labels	$Accu_y$	$Prec_n$	$Reca_l$	F_{score}	**MCC**
Training Phase (80%)					
Healthy	99.67	99.01	100.00	99.50	99.25
EGC	99.50	99.75	98.75	99.24	98.87
AGC	99.83	99.75	99.75	99.75	99.63
Average	**99.67**	**99.50**	**99.50**	**99.50**	**99.25**
Testing Phase (20%)					
Healthy	99.33	98.04	100.00	99.01	98.52
EGC	98.67	98.02	98.02	98.02	97.01
AGC	99.33	100.00	97.98	98.98	98.50
Average	**99.11**	**98.69**	**98.67**	**98.67**	**98.01**

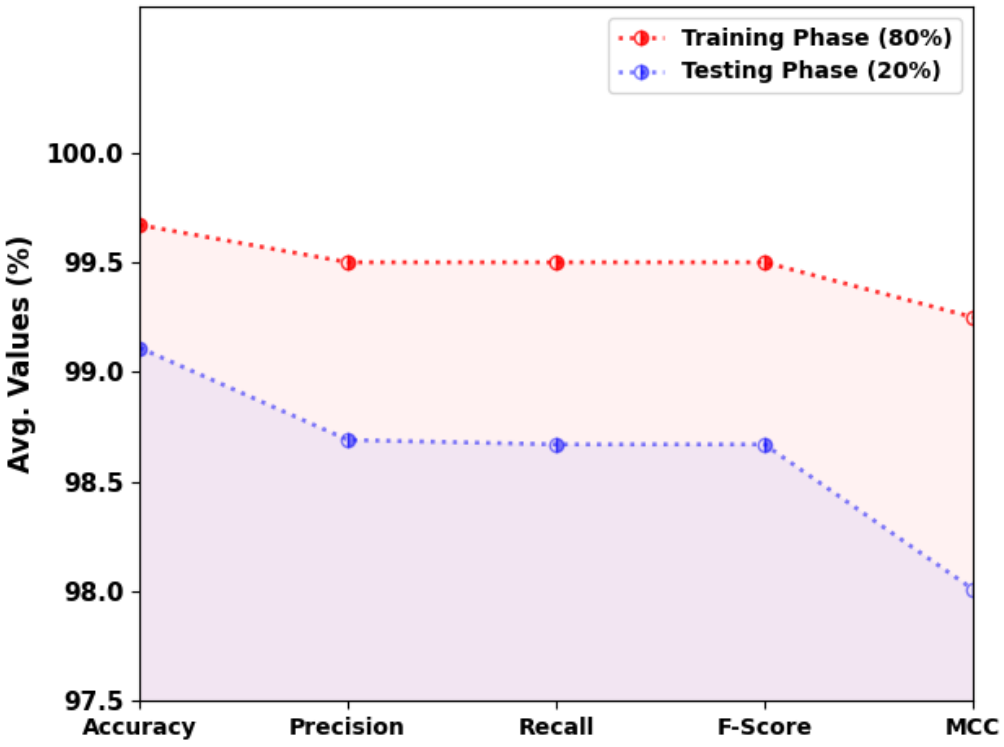

Figure 5. Average outcomes of the APODL-GCC system on 80:20 of TR/TS databases.

Table 3 and Figure 6 showcase the GC classification results achieved by the proposed APODL-GCC approach with 70: 30 of TR/TS databases. The experimental outcomes infer that the APODL-GCC approach recognized both healthy and GC cases accurately. On 70% of TR database, the APODL-GCC method reached an average $accu_y$ of 97.84%, $prec_n$ of 96.81%, $reca_l$ of 96.76%, F_{score} of 96.77%, and an MCC of 95.17%. In the meantime, on 30% of TS database, the APODL-GCC method attained an average $accu_y$ of 98.67%, $prec_n$ of 98.03%, $reca_l$ of 98%, F_{score} of 97.97%, and an MCC of 97.03%.

Table 3. GC classification outcomes of the APODL-GCC system on 70:30 of TR/TS databases.

Labels	Accuracy	Precision	Recall	F-Score	MCC
Training Phase (70%)					
Healthy	97.52	94.84	98.03	96.41	94.55
EGC	97.43	97.65	94.59	96.09	94.20
AGC	98.57	97.95	97.67	97.81	96.75
Average	**97.84**	**96.81**	**96.76**	**96.77**	**95.17**
Testing Phase (30%)					
Healthy	98.22	94.74	100.00	97.30	96.05
EGC	98.22	100.00	94.63	97.24	96.01
AGC	99.56	99.36	99.36	99.36	99.02
Average	**98.67**	**98.03**	**98.00**	**97.97**	**97.03**

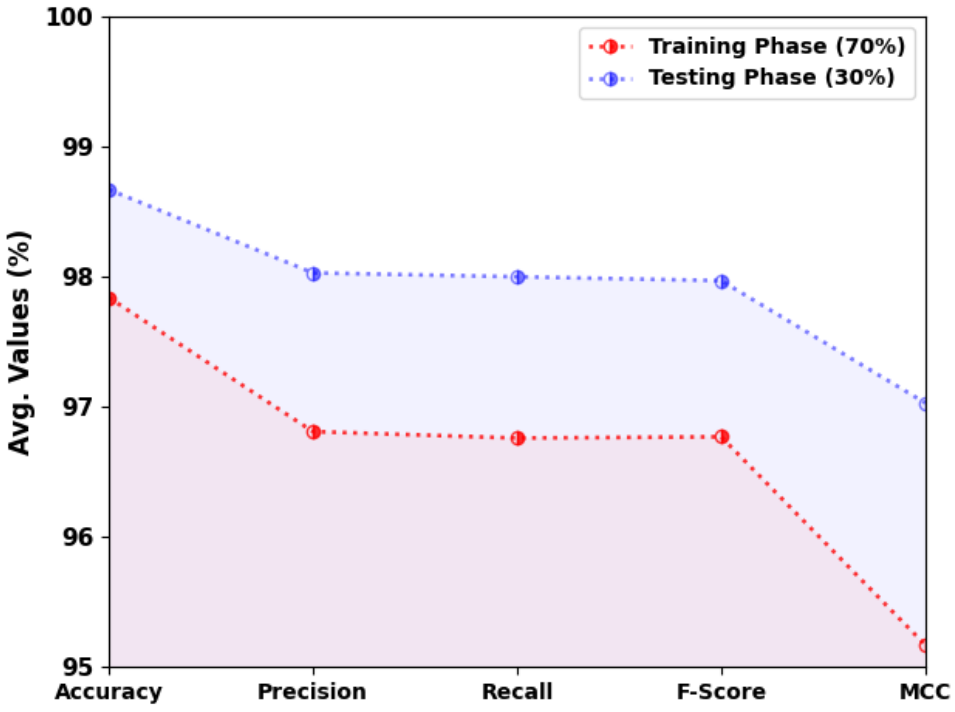

Figure 6. Average outcomes of the APODL-GCC system on 70:30 of TR/TS databases.

The TACC and VACC values, obtained by the proposed APODL-GCC technique in terms of GC classification, are shown in Figure 7. The figure shows that the APODL-GCC approach exhibited an improved performance with increased TACC and VACC values. Notably, the APODL-GCC technique reached the maximum TACC outcomes.

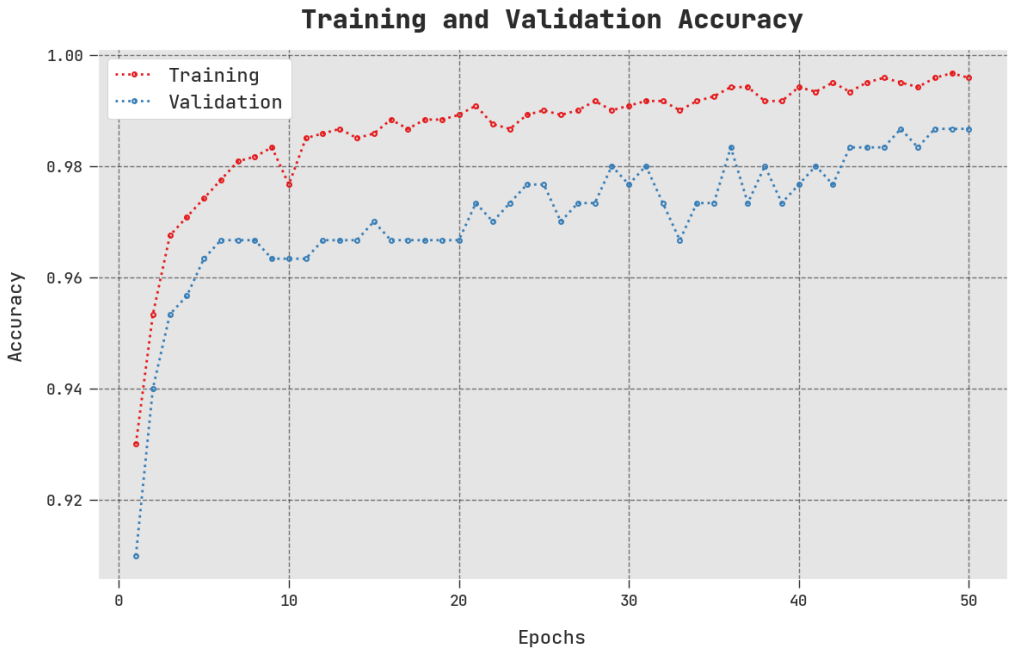

Figure 7. TACC and VACC outcomes of the APODL-GCC system.

The TLS and VLS values, accomplished by the proposed APODL-GCC approach in terms of GC classification, are portrayed in Figure 8. The figure infers that the APODL-GCC technique achieved better performance with minimal TLS and VLS values. Seemingly, the APODL-GCC approach produced low VLS outcomes.

Figure 8. TLS and VLS outcomes of the APODL-GCC system.

A clear precision-recall inspection was conducted upon the APODL-GCC approach using the test database and the results are shown in Figure 9. The figure exhibits that the APODL-GCC technique achieved enhanced precision-recall values under all the classes.

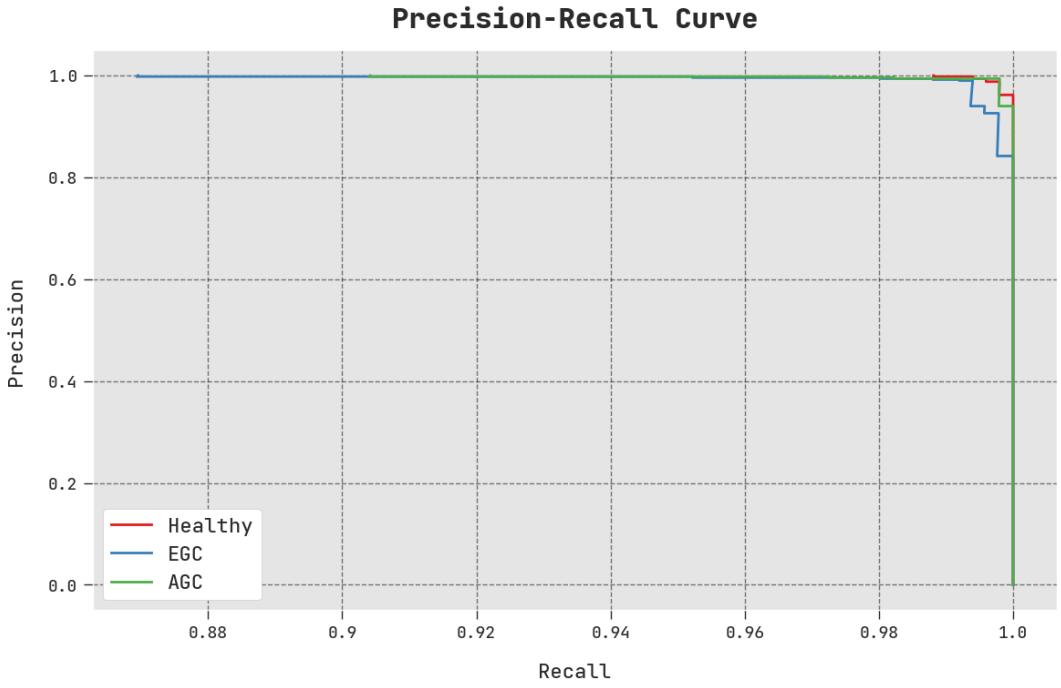

Figure 9. Precision-recall outcomes of APODL-GCC technique.

The GC classification outcomes of the APODL-GCC technique were compared with that of the results achieved by the existing DL methods and the results are shown in Table 4 and Figure 10 [26]. The outcomes found the close performance of the existing models such as SSD, CNN, and Mask R-CNN models with $accu_y$ values being 96.22, 96.77, and 96.97% respectively. Concurrently, the U-Net-CNN method and the cascade CNN method obtained moderately improved $accu_y$ values such as 98.21 and 97.07% respectively.

Table 4. Comparative analysis outcomes of the APODL-GCC technique and other recent DL methods.

Methods	$Accu_y$	$Prec_n$	$Reca_l$	F_{score}
APODL-GCC	99.67	99.5	99.5	99.50
MRFOTL-GCDC	99.17	98.42	98.96	99.13
SSD	96.22	95.53	95.61	96.28
CNN	96.77	94.94	97.77	97.55
Mask R-CNN	96.97	96.95	98.35	97.66
U-Net-CNN	98.21	97.25	97.65	95.44
Cascade CNN	97.07	96.60	97.26	97.06

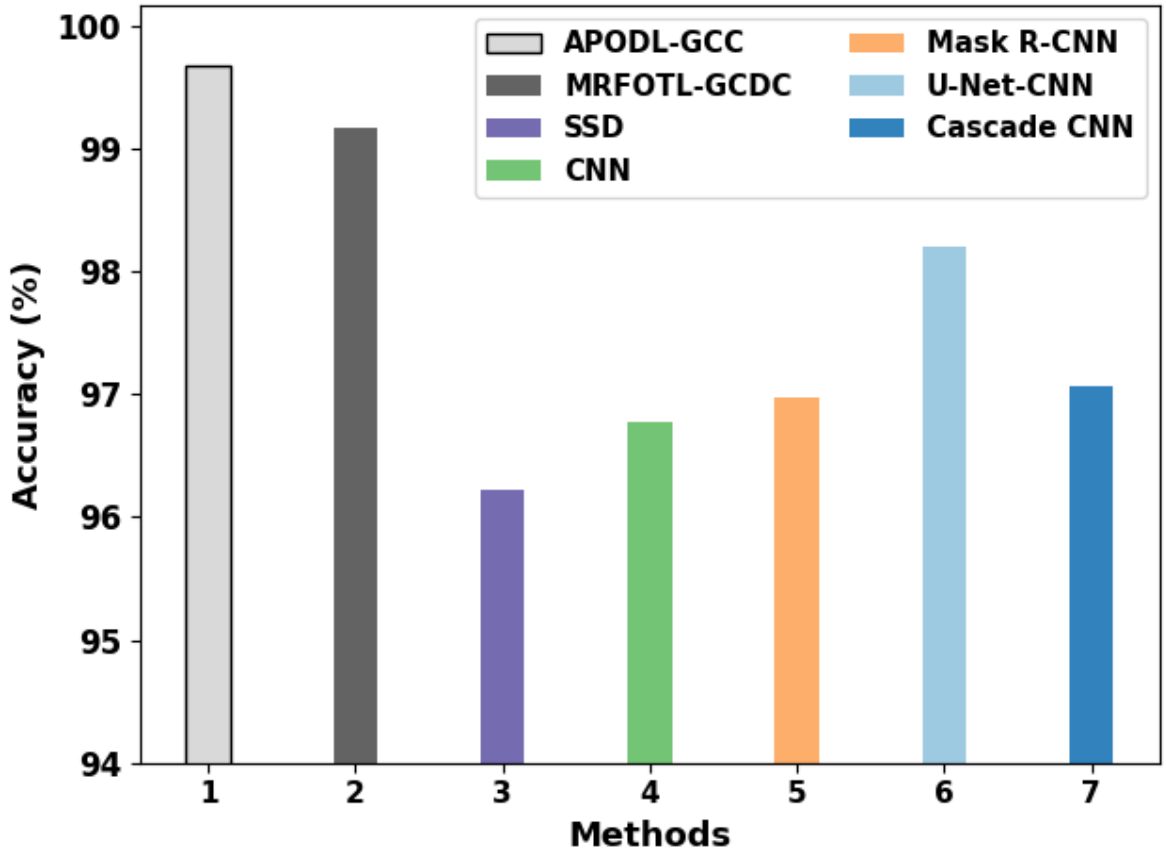

Figure 10. $Accu_y$ analysis outcomes of the APODL-GCC approach and other recent DL techniques.

On the contrary, the MRFOTL-GCDC technique managed to achieve a considerable GC classifier outcome with an $accu_y$ of 99.17. However, the proposed APODL-GCC model obtained the maximum performance, in terms of GC classification, with an $accu_y$ of 99.67%. Therefore, the APODL-GCC model can be employed in the near future for accurate GC classification.

5. Conclusions

In the current research work, a new APODL-GCC approach has been developed for GC classification on endoscopy images. The presented APODL-GCC method focuses on the identification of the GC using both CV and DL concepts. Primarily, the APODL-GCC technique employs a contrast enhancement technique. Next, the feature extraction process is performed with the help of the NASNet model to generate a collection of feature vectors. For hyperparameter optimization, the APO algorithm is used which in turn enhances the classification performance. Finally, the GC classification process is executed by the DBN model. The proposed APODL-GCC technique was simulated using the medical images. The experimental results confirmed that the proposed APODL-GCC technique accomplished an enhanced performance over other models. Therefore, the proposed model can be employed in real-time GC detection and classification tasks, which will help the physicians in decision making process. In the future, the performance of the APODL-GCC method can be boosted by the ensemble learning models.

Acknowledgments

The authors extend their appreciation to the Deputyship for Research & Innovation, Ministry of Education in Saudi Arabia for funding this research work through the project no. (IFKSURG-1742).

Conflict of interest

The authors declare that they have no conflict of interest. The manuscript was written through contributions of all authors. All authors have given approval to the final version of the manuscript.

References

1. Z. Song, S. Zou, W. Zhou, Y. Huang, L. Shao, J. Yuan, et al., Clinically applicable histopathological diagnosis system for gastric cancer detection using deep learning, *Nat. Commun.*, **11** (2020), 1–9. https://doi.org/10.1038/s41467-020-18147-8
2. Y. Zhao, B. Hu, Y. Wang, X. Yin, Y. Jiang, X. Zhu, Identification of gastric cancer with convolutional neural networks: a systematic review, *Multimedia Tools Appl.*, (2022), 1–20. https://doi.org/10.1007/s11042-022-12258-8
3. L. Zhang, D. Dong, W. Zhang, X. Hao, M. Fang, S. Wang, et al., A deep learning risk prediction model for overall survival in patients with gastric cancer: A multicenter study, *Radiother. Oncol.*, **150** (2020), 73–80. https://doi.org/10.1016/j.radonc.2020.06.010
4. X. Wang, Y. Chen, Y. Gao, H. Zhang, Z. Guan, Z. Dong, et al., Predicting gastric cancer outcome from resected lymph node histopathology images using deep learning, *Nat. Commun.*, **12** (2021), 1–13. https://doi.org/10.1038/s41467-021-21674-7
5. Z. Song, S. Zou, W. Zhou, Y. Huang, L. Shao, J. Yuan, et al., Clinically applicable histopathological diagnosis system for gastric cancer detection using deep learning, *Nat. Commun.*, **11** (2020), 1–9. https://doi.org/10.1038/s41467-020-18147-8
6. S. Ai, C. Li, X. Li, T. Jiang, M. Grzegorzek, C. Sun, et al., A state-of-the-art review for gastric histopathology image analysis approaches and future development, *BioMed. Res. Int.*, 2021. https://doi.org/10.1155/2021/6671417
7. H. Chen, C. Li, G. Wang, X. Li, M. Rahaman, H. Sun, et al., GasHis-Transformer: A multi-scale visual transformer approach for gastric histopathological image detection, *Pattern Recognit.*, **130** (2022), 108827. https://doi.org/10.1016/j.patcog.2022.108827
8. Y. Li, X. Wu, C. Li, X. Li, H. Chen, C. Sun, et al., A hierarchical conditional random field-based attention mechanism approach for gastric histopathology image classification, *Appl. Intell.*, (2022), 1–22.
9. Y. Li, C. Li, X. Li, K. Wang, M. Rahaman, C. Sun, et al., A comprehensive review of Markov random field and conditional random field approaches in pathology image analysis, *Arch. Comput. Methods Eng.*, **29** (2022), 609–639. https://doi.org/10.1007/s11831-021-09591-w
10. J. Zhang, C. Li, S. Kosov, M. Grzegorzek, K. Shirahama, T. Jiang, et al., LCU-Net: A novel low-cost U-Net for environmental microorganism image segmentation, *Pattern Recognit.*, **115** (2021), 107885. https://doi.org/10.1016/j.patcog.2021.107885
11. P. Dell'Aversana, Reservoir prescriptive management combining electric resistivity tomography and machine learning, *AIMS Geosci.*, **7** (2021), 138–161. https://doi.org/10.3934/geosci.2021009

12. S. Zhou, J. Zheng, C. Jia, SPREAD: An ensemble predictor based on DNA autoencoder framework for discriminating promoters in Pseudomonas aeruginosa, *Math. Biosci. Eng.*, **19** (2022), 13294–13305. https://doi.org/10.3934/mbe.2022622
13. J. Zhang, C. Li, Y. Yin, J. Zhang, M. Grzegorzek, Applications of artificial neural networks in microorganism image analysis: a comprehensive review from conventional multilayer perceptron to popular convolutional neural network and potential visual transformer, *Artif. Intell. Rev.*, (2022), 1–58. https://doi.org/10.1007/s10462-022-10192-7
14. F. Kulwa, C. Li, J. Zhang, K. Shirahama, S. Kosov, X. Zhao, et al., A new pairwise deep learning feature for environmental microorganism image analysis, *Environ. Sci. Pollut. Res.*, (2022), 1–18. https://doi.org/10.1007/s11356-022-18849-0
15. A. Chen, C. Li, S. Zou, M. Rahaman, Y. Yao, H. Chen, et al., SVIA dataset: A new dataset of microscopic videos and images for computer-aided sperm analysis, *Biocybern. Biomed. Eng.*, **42** (2022), 204–214. https://doi.org/10.1016/j.bbe.2021.12.010
16. W. Hu, C. Li, X. Li, M. Rahaman, J. Ma, Y. Zhang, et al., GasHisSDB: A new gastric histopathology image dataset for computer aided diagnosis of gastric cancer, *Comput. Biol. Med.*, **142** (2022), 105207. https://doi.org/10.1016/j.compbiomed.2021.105207
17. Y. Hu, L. Zhao, Z. Li, X. Dong, T. Xu, Y. Zhao, Classifying the multi-omics data of gastric cancer using a deep feature selection method, *Expert Syst. Appl.*, **200** (2022), 116813. https://doi.org/10.1016/j.eswa.2022.116813
18. Y. Li, X. Xie, S. Liu, X. Li, L. Shen, November. Gt-net: a deep learning network for gastric tumor diagnosis, in *2018 IEEE 30th International Conference on Tools with Artificial Intelligence (ICTAI)*, (2018), 20–24.
19. Y. Zhu, Q. Wang, M. Xu, Z. Zhang, J. Cheng, Y. Zhong, et al., Application of convolutional neural network in the diagnosis of the invasion depth of gastric cancer based on conventional endoscopy, *Gastrointest. Endosc.*, **89** (2019), 806–815. https://doi.org/10.1016/j.gie.2018.11.011
20. S. Lee, H. Cho, H. Cho, A novel approach for increased convolutional neural network performance in gastric-cancer classification using endoscopic images, *IEEE Access*, **9 (**2021), 51847–51854. https://doi.org/10.1016/j.gie.2018.11.011
21. H. Yoon, S. Kim, J. Kim, J. Keum, S. Oh, J. Jo, et al., A lesion-based convolutional neural network improves endoscopic detection and depth prediction of early gastric cancer, *J. Clin. Med. Res.*, **8** (2019), 1310. https://doi.org/10.3390/jcm8091310
22. X. Liu, C. Wang, Y. Hu, Z. Zeng, J. Bai, G. Liao, Transfer learning with convolutional neural network for early gastric cancer classification on magnifiying narrow-band imaging images, in *2018 25th IEEE International Conference on Image Processing (ICIP)*, (2018), 1388–1392. https://doi.org/10.1109/ICIP.2018.8451067
23. A. Adedoja, P. Owolawi, T. Mapayi, Deep learning based on nasnet for plant disease recognition using leave images, in *2019 International Conference on Advances in Big Data, Computing and Data Communication Systems (icABCD)*, (2019), 1–5. https://doi.org/10.1109/ICABCD.2019.8851029
24. Y. Zhang, P. Wang, L. Yang, Y. Liu, Y. Lu, X. Zhu, Novel swarm intelligence algorithm for global optimization and multi-UAVs cooperative path planning: Anas platyrhynchos optimizer, *Appl. Sci.*, **10** (2020), 4821. https://doi.org/10.3390/app10144821
25. J. Wan, B. Chen, Y. Kong, X. Ma, Y. Yu, An early intestinal cancer prediction algorithm based on deep belief network, *Sci. Rep.*, **9 (**2019), 1–13. https://doi.org/10.1038/s41598-018-37186-2

26. F. Alrowais, S. Alotaibi, R. Marzouk, A. Salama, M. Rizwanullah, A. Zamani, et al., Manta ray foraging optimization transfer learning-based gastric cancer diagnosis and classification on endoscopic tmages, *Cancers*, **14** (2022), 5661. https://doi.org/10.3390/cancers14225661

AIMS Press